Aalto University

OPEN ACCESS

This is an electronic reprint of the original article.
This reprint may differ from the original in pagination and typographic detail.

Kivisaari, Pyry; Chen, Yang; Anttu, Nicklas

Emission enhancement, light extraction and carrier dynamics in InGaAs/GaAs nanowire arrays

Published in:
NANO FUTURES

DOI:
10.1088/2399-1984/aaa666

Published: 01/01/2018

Document Version
Peer-reviewed accepted author manuscript, also known as Final accepted manuscript or Post-print

Please cite the original version:
Kivisaari, P., Chen, Y., & Anttu, N. (2018). Emission enhancement, light extraction and carrier dynamics in InGaAs/GaAs nanowire arrays. *NANO FUTURES*, *2*(1), 1-9. Article 015001. https://doi.org/10.1088/2399-1984/aaa666

This material is protected by copyright and other intellectual property rights, and duplication or sale of all or part of any of the repository collections is not permitted, except that material may be duplicated by you for your research use or educational purposes in electronic or print form. You must obtain permission for any other use. Electronic or print copies may not be offered, whether for sale or otherwise to anyone who is not an authorised user.

Emission enhancement, light extraction and carrier dynamics in InGaAs/GaAs nanowire arrays

Pyry Kivisaari
Division of Solid State Physics and NanoLund, Lund University, P.O. Box 118, SE-22100 Lund, Sweden and Engineered Nanosystems Group, Aalto University, P.O. Box 12200, FI-00076 Aalto, Finland

Yang Chen
Division of Solid State Physics and NanoLund, Lund University, P.O. Box 118, SE-22100 Lund, Sweden

Nicklas Anttu
Department of Electronics and Nanoengineering, Aalto University, P.O. Box 13500, FI-00076 Aalto, Finland.

Nanowires (NWs) have potential for a wide range of new optoelectronic applications. For example, light-emitting diodes that span over the whole visible spectrum are currently being developed from NWs to overcome the well known green gap problem. However, due to their small size, NW devices exhibit special properties that complicate their analysis, characterization, and further development. In this paper, we develop a full optoelectronic simulation tool for NW array light emitters accounting for carrier transport and wave-optical emission enhancement, and we use the model to simulate InGaAs/GaAs NW array light emitters with different geometries and temperatures. Our results show that NW arrays emit light preferentially to certain angles depending on the NW diameter and temperature, encouraging temperature- and angle-resolved measurements of NW array light emission. On the other hand, based on our results both the emission enhancement and light extraction efficiency can easily change by at least a factor of two between room temperature and 77 K, complicating the characterization of NW light emitters if conventional methods are used. Finally, simulations accounting for surface recombination emphasize its major effect on the device performance. For example, a surface recombination velocity of 10^4 cm/s reported earlier for bare InGaAs surfaces results in internal quantum efficiencies less than 30 % for small-diameter NWs even at the temperature of 30 K. This highlights that core-shell structures or high-quality passivation techniques are eventually needed to achieve efficient NW-based light emitters.

Keywords: semiconductor, nanowire array, light-emitting diodes, light extraction, emission enhancement, surface recombination

I. INTRODUCTION

Nanowires (NWs) are expected to enable several new application areas for light-emitting diodes (LEDs). For example, nitride NWs have been used to create full red-green-blue (RGB) display technologies [1], and the recently demonstrated NW-based ternary nitride templates may finally enable creating efficient white-light LED lighting without the need for lossy phosphors [2]. Moreover, due to special strain-relaxation properties of NWs, III-V growth on silicon is much more straightforward with NWs than with bulk growth, making NWs a highly viable building block for light emitters in future silicon photonics [3]. NW-based light emitters/absorbers have also been suggested to enable a wide range of new optical biosensing applications to complement today's electrostatic sensor technologies [4].

Because of their nanoscale dimensions and hence special optical and electrical properties, design and analysis of NW light emitters is challenging. NW light emitters show strongly geometry-dependent optical properties like suppressed/enhanced [5, 6], directional [7, 8], and polarized [7, 8] emission. In a recent work we calculated emission characteristics of NW array light-emitting diodes using full wave-optical modeling [5]. We found that the emission enhancement (EE) and light extraction efficiency (LEE) of NW array LEDs depend strongly on the NW diameter due to the presence of resonant modes. On the electrical side, especially surface recombination introduces strong geometry dependence into the NW LED performance [9]. Kölper *et al.* performed full-device modeling of III-N NW LEDs by coupling finite difference-time domain (FDTD) simulations of EE and LEE to a carrier-density based model of the quantum efficiency [10]. In addition, Wang et al. developed advanced and computationally demanding fully coupled optoelectronic models for NW solar cells which also accounted for spontaneous emission and photon recycling [11].

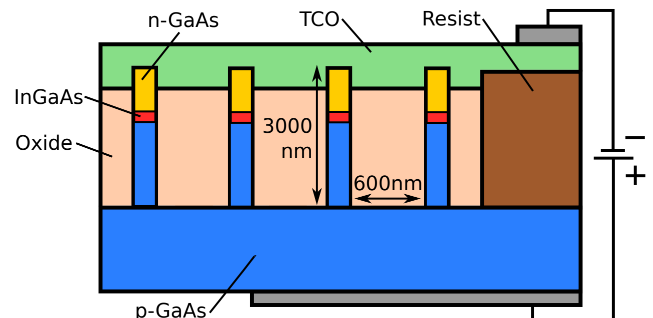

FIG. 1. The nanowire array LED device simulated in this paper.

However, future design and analysis of NW-array LEDs requires dedicated studies of their optical and electrical aspects. In this paper we show that accounting for the interplay between nano-optics and carrier dynamics is necessary for understanding new NW-based light emitters. We develop and carry out full opto-electronic simulations of NW array LEDs,

calculating the Purcell factor (defined as the modification of the EE relative to that in a bulk homogeneous material) and LEE from wave optics and incorporating them in the carrier transport modeling. The simulations are performed for the NW array structure shown in Figure 1 at different temperatures ranging from 4K to 300K. The 3000 nm long NWs stand on a p-type GaAs substrate in a square array with a pitch of 600 nm, and the NW diameter is varied between 20 and 840 nm. The low-bandgap active region (AR) consists of an axial InGaAs segment of 10 nm in thickness.

Our results show that the emission pattern of such NW arrays exhibits strong angle dependence if the NWs are sufficiently thin. Moreover, due to the temperature dependence of the emission wavelength, the emission pattern changes drastically as a function of temperature. Consequently, also the EE and LEE depend strongly on temperature, in contrast to what is assumed in the low-temperature characterization of typical planar LEDs [12, 13]. Supplemented with the optics results, full-device simulations show that in the device structure chosen for the analysis, neglecting the temperature dependence of EE and LEE results in an error of over 20 percentage points in the internal quantum efficiency (IQE). We also show that surface recombination ruins the IQE of NW light emitters at small diameters even at very low temperatures, emphasizing the need for core-shell structures or high-quality surface passivation techniques.

II. THEORETICAL TOOLS

We model the EE and LEE with the Maxwell equations, similarly as in Ref. 5. Here, we extend the optics study to include spatial dependence of the EE and LEE for emission from varying location along the axis of the NWs, and we study also the angular dependence of the EE. As input for the optics modeling, we use the refractive index of the materials and the geometry of the LED. Specifically, from the optics modeling, by integrating the EE over all emission angles to the top air side and into the substrate, we obtain the Purcell factor γ_{Pur} that is the modification of the emission rate relative to that in the corresponding bulk material. Also, we obtain the fraction of photons emitted to the top air side P_{top}, as well as into the substrate P_{subs}, from which the LEE is obtained as LEE $= P_{top}/(P_{top}+P_{subs})$. Note that in our structure, no bound (or guided) radiative modes exist in the plane of the array due to the high refractive index substrate, and hence all emitted photons couple either to the top or the bottom side of the structure. Note also that for simplicity and due to the small size of the low-bandgap AR, we neglect re-absorption of emitted photons. More details are given in the Supporting Information.

The charge transport and recombination in the nanowires is modeled using the drift-diffusion model given by [14]

$$\begin{aligned} \nabla\cdot(-\varepsilon\nabla\phi) &= e\left(p-n+N_d-N_a\right) \\ \nabla\cdot\mathbf{J}_n = \nabla\cdot(-e\mu_n n\nabla\phi_n) &= eR \\ \nabla\cdot\mathbf{J}_p = \nabla\cdot(-e\mu_p p\nabla\phi_p) &= -eR, \end{aligned} \quad (1)$$

where ε is the static permittivity of the medium, e is the elementary charge, n,p are the electron and hole densities, N_d,N_a are the ionized donor and acceptor densities, $\mathbf{J}_n,\mathbf{J}_p$ are the electron and hole current densities, μ_n,μ_p are the electron and hole mobilities, and R is the net recombination rate density including radiative and nonradiative processes. 3D carrier statistics are assumed throughout the device for simplicity, and the equation system is solved self-consistently to give steady-state solutions for the electrostatic potential ϕ and the quasi-Fermi potentials ϕ_n,ϕ_p for electrons and holes, respectively. Note that the recombination rates and electron and hole densities also depend on the fields that are solved for. More details on the model including the required boundary conditions and constitutive relations are given in Ref. 15.

All the recombination processes have temperature dependences, and radiative recombination furthermore depends on the local optical density of states as previously described. To elaborate on the nano-optical effects on radiative recombination and effects of temperature on all the recombination processes, we write the total bulk recombination rate as [16]

$$R = R_{srh}+R_{rad}+R_{aug} =$$

$$\left(\frac{1}{\tau_p(n+n_1)+\tau_n(p+p_1)}+\gamma_{Pur}B+C(n+p)\right)\left(np-n_i^2\right), \quad (2)$$

where the total bulk recombination is the sum of nonradiative Shockley-Read-Hall (SRH), bimolecular radiative and Auger recombination. Furthermore, τ_p is the SRH lifetime of holes assuming a large density of electrons and τ_n is the corresponding SRH lifetime of electrons, n_1 and p_1 are the electron and hole densities when the Fermi level coincides with the trap level causing the SRH recombination, n_i is the intrinsic carrier concentration, γ_{Pur} is the Purcell factor describing EE, B is the net radiative recombination coefficient for bulk, and C is the Auger recombination coefficient assuming an equal coefficient for *nnp* and *npp* Auger processes.

The radiative recombination model of Eq. (2) is based on assuming that (i) spontaneous emission is dominated by direct transitions between parabolic conduction and valence bands and (ii) Boltzmann approximation can be used [16]. According to Refs. [16, 17], the radiative recombination coefficient in this case depends on temperature as $B(T)=B_0(T/300\text{K})^{-3/2}$, where B_0 is the value of B at 300 K. In other words, the radiative recombination coefficient increases as temperature decreases. On the other hand, according to the original paper by Shockley and Read [18], the SRH lifetimes τ_n and τ_p do not have significant temperature dependence, and therefore the SRH temperature dependence results primarily from the temperature dependence of n_1, p_1 and n_i. For the temperature dependence of Auger recombination, we use a model where the Auger coefficient C depends on temperature as

$$C(T) = C_0\exp\left[\frac{\hbar\omega_q}{k}\left(\frac{1}{300\text{K}}-\frac{1}{T}\right)\right], \quad (3)$$

where C_0 is C at 300 K and ω_q is the optical phonon frequency, resulting from the theory of indirect phonon-assisted Auger

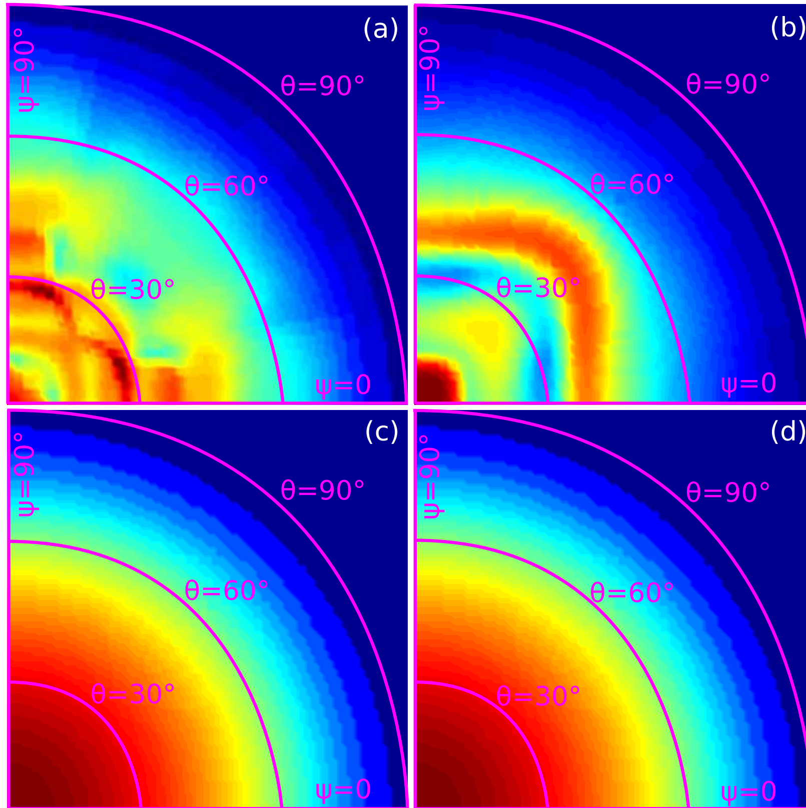

FIG. 2. Emission enhancement (EE) towards the top side of the NW array LED as a function of the polar angle (θ) and the azimuthal angle (ψ) with (a) NW diameter of 310 nm and temperature 300 K, (b) NW diameter 300 nm and temperature 77 K, (c) NW diameter 840 nm and temperature 300K, and (d) NW diameter 840 nm and temperature 77 K, averaged over polarization. Note that $\theta = 0$ corresponds to normally incident light, that is, light incident parallel to the NW axis, and $\psi = 0$ corresponds to an incidence plane that is parallel to a symmetry axis of the square array where neighboring nanowires are separated by the pitch of 600 nm. The 10 nm thick AR is located 100 nm away from the NW top surface.

processes [16]. In our model the Auger recombination therefore decreases as temperature decreases, whereas the SRH recombination is only weakly dependent on temperature, similarly as reported for InAs from full band structure calculations [19].

Due to the large surface-to-volume ratio of NWs, surface recombination has to be taken into account in the modeling of InGaAs/GaAs NWs [20]. In our simulations, we employ the model of SRH-like surface recombination based on Refs. [15, 21]. Furthermore, to enable 1D charge transport simulations of 3-dimensional NWs, we transform the surface recombination velocity into an effective bulk SRH recombination parameter similarly as in our recent work [22]. As surface recombination is also an SRH-like process, we assume that the surface recombination velocity has no dependence on temperature as was the case also for the SRH lifetimes in the previous paragraph.

To account for other temperature dependences, the bandgap is calculated as a function of temperature using the Varshni formulation given by $E_g(T) = E_g(T=0) - \alpha T^2/(T+\beta)$, where α and β are the Varshni parameters [23]. For the temperature dependence of the refractive index, we use tabulated data for GaAs with interpolation and extrapolation to the values at varying wavelength and temperature in Ref. 24. Note that we use the values for GaAs also for the thin InGaAs AR segment, since the InGaAs segment is so thin that the difference in refractive index causes negligible optical effects. The static dielectric constant and electron/hole mobility follow the temperature dependences as given in Ref. 25. The static permittivity is given by $\varepsilon_r = \varepsilon_{r,0}(1+1.2\times10^{-4}T)$, where $\varepsilon_{r,0}$ and ξ are constants. The electron/hole mobilities are interpolated from the temperature dependences reported in Ref. 25. All the required material and simulation parameters are listed in the Supporting Information.

Note that we do not consider mirrors and packaging that would eventually be needed for efficient devices. On the other hand, we assume that all the photons emitted into the substrate are lost, as would normally be the case in a laboratory prototype LED. Due to this reason, also the simulated LEEs and external quantum efficiencies (EQEs) are much lower than in industrial LEDs, making our results especially well suited for NW array light emitters at their early development stages. We choose the composition of the InGaAs in the AR to correspond to a band-to-band emission wavelength of 1310 nm at 300 K, which shifts to 1215 nm at 77 K and 1204 nm at 30 K, as calculated using the Varshni formulation.

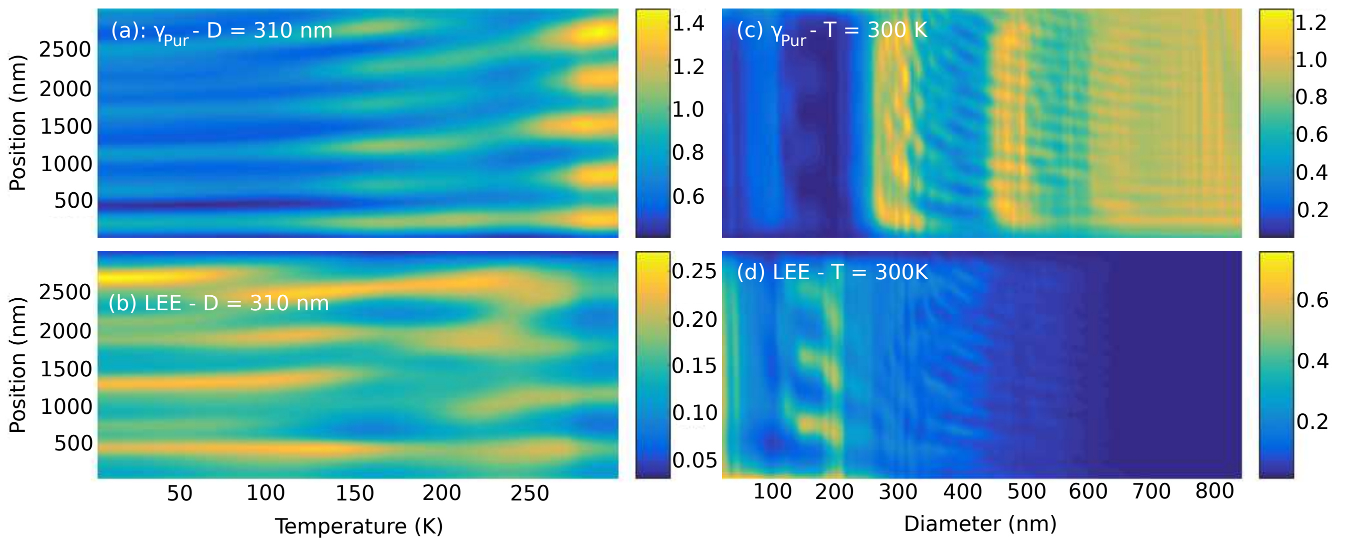

FIG. 3. (a) Purcell factor and (b) LEE as a function of the position of the AR within the NW and temperature for a NW diameter of 310 nm, and (c) Purcell factor and (d) LEE as a function of the position of the AR within the NW and diameter for a temperature of 300 K. The position is 0 at the NW top surface and 3000 at the substrate.

III. RESULTS & DISCUSSION

Full optoelectronic simulations were carried out for the NW structures of Figure 1. We begin here with results from the optical modeling and continue with the coupled full device modeling results. Figure 2 shows angle-resolved EE into the top side of the NWs as a function of the emission angle. The NW diameters are (a,b) 310 nm and (c,d) 840 nm and the temperatures are (a,c) 300 K and (b,d) 77 K. In Figure 2, the AR is located 100 nm from the NW top surface. Due to wave-optical effects and the non-isotropic NW array structure, the EE shows strong angle dependence both in the polar and azimuthal directions. In Figure 2(a), the NWs with diameter $D = 310$ nm emit most strongly towards a polar angle close to 30° at $T = 300$ K. On the other hand, in Figure 2(b) at $T = 77$ K, the same LED shows a drastically different emission pattern due to the modified emission wavelength, and the emission peaks at a polar angle of roughly 0 degrees. This suggests that temperature-controlled angle-resolved measurements of axial NW LED structures could give very valuable insight on the optical response of the structure. More importantly, these results also suggest that the overall EE and LEE depend on the temperature. Figures 2(c,d) show that as the NW diameter is increased to 840 nm where the NWs have merged into an almost continuous film (which occurs at $\sqrt{2} \times 600$ nm ≈ 849 nm), special angle dependences vanish and the emission pattern starts to resemble a typical Lambertian pattern.

To get a more complete picture on the nano-optics of the NW arrays, Figure 3 shows the Purcell factors and LEEs within a single NW in the array at different temperatures and diameters. In Figure 3(a), we show the Purcell factor as a function of the position of the AR within the NW and temperature, assuming a NW diameter of 310 nm. This diameter is chosen since it supports a resonant mode at 300 K that gives the strong peaks in the Purcell factor at that temperature in the right-hand side of Figure 3(a). However, as the temperature decreases and as the emission wavelength thereby changes, the emission shifts away from resonant excitation of the mode, and the Purcell factor decreases strongly. In the LEE for the same diameter in Figure 3(b), on the other hand, we also see a strong dependence on the temperature. Note that the LEE shows minima at 300 K at the spots where the Purcell factor shows maxima in Figure 3(a), indicating that the EE is enhanced primarily by emission into the substrate. This suggests that applicable mirrors and packaging are needed even in NW array LEDs to enhance their light extraction.

The dependence of the Purcell factor and LEE on the NW diameter is illustrated in Figures 3(c,d). In Figure 3(c), we see that NWs with a diameter less than 300 nm have Purcell factors much less than 1, corresponding to strong emission suppression. On the other hand, the Purcell factor shows two clear regimes where it obtains high values, namely around the diameters of 300 nm and 500 nm due to modes in the NWs that couple efficiently to freely propagating light above and/or below the NWs. As the diameter approaches large values, the Purcell factor approaches unity as expected, as the structure starts to resemble a homogeneous planar device.

The LEE shown in Figure 3(d) shows its highest values at diameters smaller than 300 nm where the Purcell factor had low values. In particular, in Figure 3(d) we can identify the peaks at roughly 180 nm, which correspond to the HE11 resonance (see, e.g., Ref. 7) that couples strongly to optical modes in air. This means that the NWs emit light primarily towards air (approximately twice as strongly as into the substrate), so that the LEE obtains large values even if the overall Purcell factor remains small. A similar trend was observed experimentally very recently by Hauswald *et al.* in Ref. 26, where they saw a decrease in the detected photoluminescence inten-

sity in GaN NWs as the NW diameter increased from 120 nm to 240 nm. According to their optics simulations, this decrease could be fully explained by a similar trend in the LEE as seen in Figure 3(d) here. Here the LEE shows rather low values at larger diameters, further highlighting that light emission is strongest towards the substrate and should eventually be utilized by, e.g., using a backreflector or flip-chip device design.

To illustrate how nano-optics affects the full device operation, we have selected some of the most interesting device geometries for full device simulation. First of all, we used the diameter of 310 nm discussed earlier and chose the position of the AR as the one corresponding to the highest Purcell factor at 300 K, that is 825 nm from the NW top surface. The Purcell factor and LEE averaged over all emission angles then were 1.26 and 0.09 at 300 K, respectively, and 0.56 and 0.15 at 77 K. The current-voltage characteristics from the device simulations are shown in Figure 4(a) for 300 K, 77 K, and 30 K, assuming zero surface recombination (corresponding to perfect surface passivation). The Purcell factor and LEE for 77 K are also used for the 30 K case, as the bandgap dependence on temperature is almost negligible at the lowest temperatures according to Varshni's model. In Figure 4(a), larger voltages are needed to drive the LED as temperature decreases, since the bandgap energy increases and carrier densities in the space-charge region decrease, as studied in more detail by Kantner and Koprucki in Ref. 27.

The EQE simulated at 300 K and at 77 K is shown in Figure 4(b) still assuming zero surface recombination, and the curve 'T = 77K, EE assumed independent of T' illustratively shows the EQE from an erroneous simulation where the same Purcell factor and LEE were used as for 300 K. Following the LEE definition used in this work, only those photons that are extracted into the air side of the device (top side in Figure 1) increase the EQE. Based on Figure 4(b), nano-optical effects and their dependence on temperature clearly need to be accounted for to make realistic temperature-dependent full-device simulations. On the other hand, the IQE of the device with $D = 310$ nm is shown in Figure 4(c) at the three different temperatures. It can be seen that without surface recombination, the maximum IQE is close to unity already at 77 K due to the enhanced radiative recombination rate and suppressed Auger recombination rate. Therefore the conventional assumption of the IQE being close to unity at low temperatures (see, e.g., Refs. [12, 13]) is in our case fulfilled already at 77 K with no surface recombination. However, to simulate a conventional measurement of the IQE, Figure 4(b) also shows an IQE estimate obtained by dividing the simulated EQE at 300 K with the simulated EQE at 77 K ('T=300K, estimated'). As the Purcell factor and LEE have changed with the temperature, the dotted curve gives an estimate for the IQE that is off by more than 20 percentage points from the real value in this specific device.

Simulations up to now have not included surface recombination. Figure 5 shows the efficiencies simulated for four different NW diameters, using the EEs and LEEs from the optical simulations and accounting for surface recombination with a modest surface recombination velocity (v_{sr}) 10^4 cm/s in

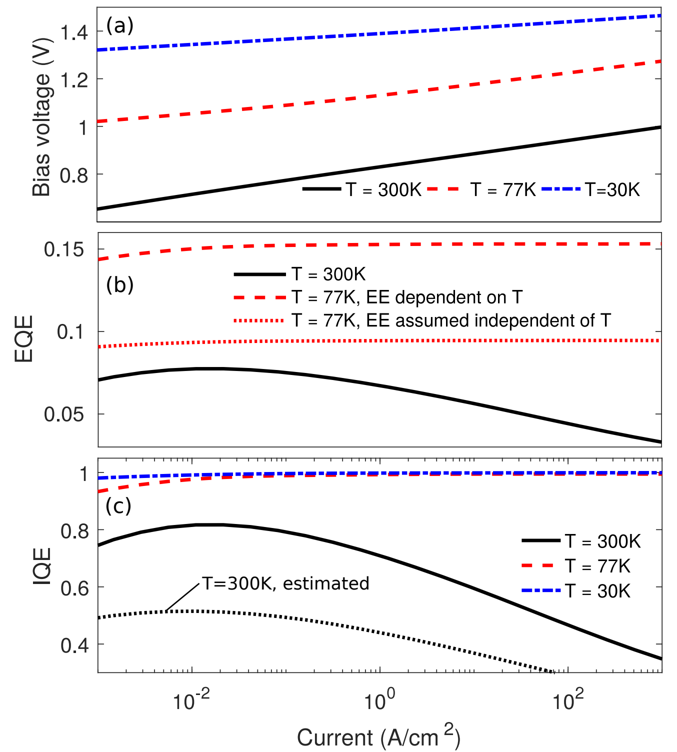

FIG. 4. (a) Bias voltage, (b) EQE and (c) IQE of the NW array LED with diameter 310 nm at 300, 77 and 30 K, assuming ideal surface passivation. The curve "T = 77K, EE assumed independent of T" in (b) is simulated using the same EE and LEE factors as in 300K. In (c), the curve "T=300K, estimate" is calculated from the simulation results as EQE(300K)/EQE(77K).

accordance with Ref. 28. First of all, Figure 5(a) shows significantly smaller IQEs than Figure 4(c), highlighting that good surface passivation is needed to make efficient NW LEDs. In addition, the maximum IQE increases as the NW diameter increases as expected, as the surface-to-volume ratio and thereby the fraction of surface recombination decreases (or in other words, the effective carrier lifetime increases for a fixed v_{sr}). On the other hand, Figure 5(a) also shows that the maximum IQE is small in all these cases. The IQE of the NW device with $D = 155$ nm is less than 1 % due to the strong emission suppression discussed earlier and a severe surface recombination due to its large surface-to-volume ratio.

The EQE of the NW devices is shown for the different NW diameters in Figure 5(b). Strikingly, it can be seen that the maximum EQE is no longer a monotonous function of the NW diameter as was the case with the IQE, since the LEE is a strongly non-monotonous function of the NW diameter. Therefore the device with $D = 310$ nm reaches the highest maximum EQE of all the devices. Note that the combined effect of the strong surface recombination and our definition of the LEE causes the maximum EQE to be only of the order of 1 % for all the devices. The IQE is shown at 30 K in Figure 5(c), and it is seen that in contrast to the case of zero surface recombination, the IQE here is notably less than unity even at 30 K. This is in line with Ref. 29, where Feix *et al.* recently ob-

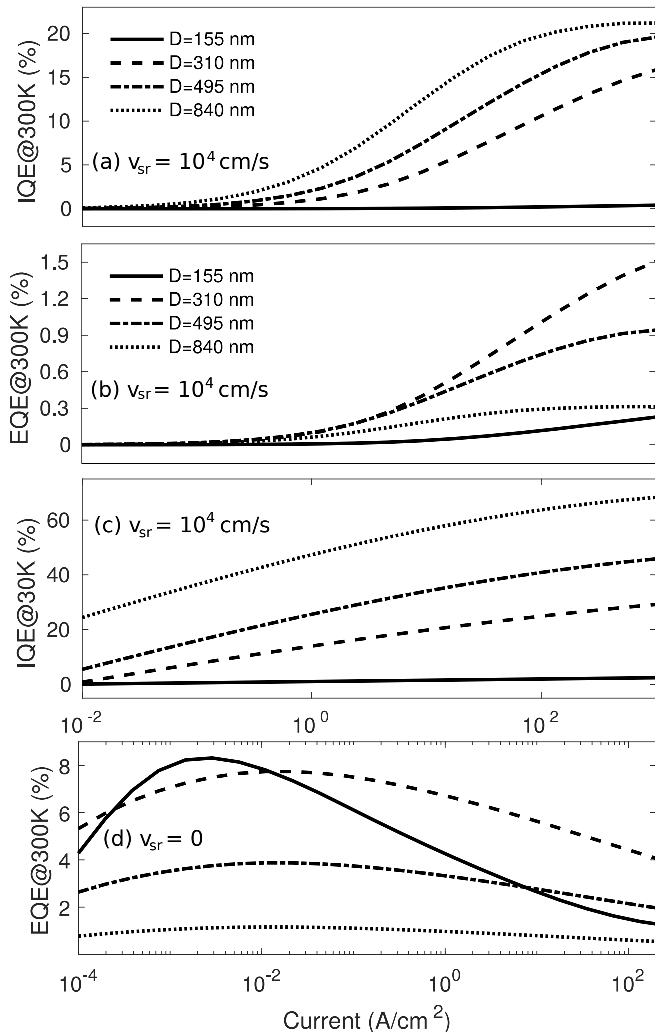

FIG. 5. Efficiencies of NW array devices with diameters 155, 310, 495 and 840 nm with a surface recombination velocity (v_{sr}) 10^4 cm/s: (a) IQE at 300K, (b) EQE at 300K and (c) IQE at 30K. For comparison, (d) shows the EQE at 300K assuming zero surface recombination. The labels given in (a) and (b) apply also in (c) and (d).

served strong nonradiative recombination in their InGaN/GaN NWs that kept the IQE of the NWs low even at 10 K. For comparison, Figure 5(d) shows the simulated EQE of the devices with different diameters with zero surface recombination. It can be seen that also in this case, the device with $D = 310$ nm shows the best performance due to its largest EE and LEE. In addition, in Figure 5(d), the maximum EQE of the device with $D = 155$ nm is comparable to the other devices due to a smaller total nonradiative rate than in Figure 5(b). However, as the Purcell factor is much less than 1 for $D = 155$ nm, the radiative recombination coefficient is also much smaller than in the other devices. This means that Auger recombination becomes larger than radiative recombination already at small currents.

To give a more concrete picture on how the value of v_{sr} affects the device performance, in Figure 6 we plot the IQE of the device with $D = 310$ nm with surface recombination

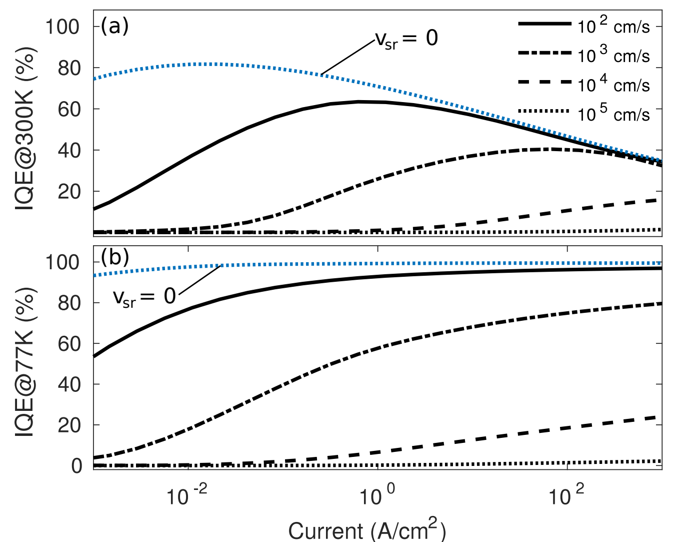

FIG. 6. IQE of the device with diameter 310 nm simulated with the surface recombination velocities listed in (a) at temperatures (a) 300 K and (b) 77 K.

velocities listed in the figure. The results are shown both for room temperature (Figure 6(a)) and that of liquid nitrogen (Figure 6(b)). In Figure 6(a) we see that the increasing surface recombination velocity decreases the peak IQE as expected. More specifically, $v_{sr} = 10^3$ cm/s already drops the peak IQE of the device to half of its value at $v_{sr} = 0$. Increasing v_{sr} and the correspondingly increasing effective SRH parameter also move the peak IQE to larger current densities in accordance with the explanations given in Ref. 30. In Figure 6(b), as the temperature decreases to 77 K, the peak IQE increases for all the values of v_{sr} as compared to 300 K due to enhanced radiative recombination and suppressed Auger recombination. However, we can see that only the IQEs with $v_{sr} = 0$ and $v_{sr} = 10^2$ cm/s reach peak values close to 100 % at the usable current density range shown in the figure. Note that based on previous Figures 5(a) and 5(c), surface recombination becomes less significant as the NW diameter increases.

The optical calculations of this paper were done assuming that the NW array and the substrate are in air. Accounting for the oxide and contact layers in Figure 1 would affect some of the quantitative details of the results but not the general observations and effects. In addition, photon recycling was not accounted for in this paper, but we expect it to have only very minor effects due to the small size of the axial AR as compared to the full structure. However, photon recycling would need to be accounted for in more complex structures with larger ARs, such as radial core-shell structures.

IV. CONCLUSIONS

In conclusion, we carried out coupled optical-electrical device simulations of NW light emitters accounting fully for nano-optical modifications in the emission enhancement and light extraction efficiency. The results showed that NWs

emit light preferentially to certain directions depending on the size of the NWs and ambient temperature, strongly motivating angle- and temperature-resolved measurements of NW light emission. Consequently, also the EE and LEE were strongly temperature-dependent, and the coupled optical-electrical simulations showed that this complicates the measurement of the IQE of NW LEDs. Finally, simulations carried out with selected surface recombination velocities showed that even a velocity of 10^4 cm/s resulted in IQEs less than 30 % at low temperatures in the small-diameter NWs. This highlights that core-shell structures or high-quality passivation techniques are needed in order to pursue efficient NW-based devices.

SUPPORTING INFORMATION

Material parameters used in the simulations as well as a detailed description of the optical model can be found in the supporting information.

ACKNOWLEDGEMENTS

Financial support from the Nokia Foundation, Emil Aaltonen Foundation and Walter Ahlström Foundation along with the People Programme (Marie Curie Actions) of the EU's 7th Framework Programme under grant agreement 608153 (PhD4Energy) is gratefully acknowledged.

[1] B. Monemar, B. J. Ohlsson, N. F. Gardner, and L. Samuelson, "Nanowire-Based Visible Light Emitters, Present Status and Outlook," *Semicond. Semimet.*, vol. 94, 227, 2016.
[2] L. Samuelson, B. Monemar, B. J. Ohlsson, and N. F. Gardner, "Gallium nitride nano-sized LEDs," *SPIE Newsroom*, 6 April, 2016. doi:10.1117/2.1201603.006385
[3] R. Yan, D. Gargas, and P. Yang, "Nanowire photonics," *Nat. Photonics*, vol. 3, 569, 2009.
[4] D. J. Sirbuly, M. Law, H. Yan, and P. Yang, "Semiconductor Nanowires for Subwavelength Photonics Integration," *J. Phys. Chem. B*, vol. 109, 15190, 2005.
[5] N. Anttu, "Modifying the emission of light from a semiconductor nanowire array," *J. Appl. Phys.*, vol. 120, 043108, 2016.
[6] R. Paniagua-Domínguez, G. Grzela, J. Gómez Rivas, and J. A. Sánchez-Gil, "Enhanced and directional emission of semiconductor nanowires tailored through leaky/guided modes," *Nanoscale*, vol. 5, 10582, 2013.
[7] D. van Dam, D. R. Abujetas, R. Paniagua-Domínguez, J. A. Sánchez-Gil, E. P. A. M. Bakkers, J. E. M. Haverkort, and J. Gómez Rivas, "Directional and Polarized Emission from Nanowire Arrays," *Nano Lett.*, vol. 15, 4557, 2015.
[8] G. Grzela, R. Paniagua-Domínguez, T. Barten, Y. Fontana, J. A. Sánchez-Gil, and J. Gómez Rivas, "Nanowire Antenna Emission," *Nano Lett.*, vol. 12, 5481, 2012.
[9] F. Römer and B. Witzigmann, "Modelling surface effects in nano wire optoelectronic devices," *J. Comput. Electron.*, vol. 11, 431, 2012.
[10] C. Kölper, M. Sabathil, F. Römer, M. Mandl, M. Strassburg, and B. Witzigmann, "Core-shell InGaN nanorod light emitting diodes: Electronic and optical device properties," *Phys. Status Solidi A*, vol. 209, 2304, 2012.
[11] X. Wang, M. R. Khan, M. Lundstrom, and P. Bermel, "Performance-limiting factors for GaAs-based single nanowire photovoltaics," *Opt. Express*, vol. 22, A344, 2014.
[12] S. Watanabe, N. Yamada, M. Nagashima, Y. Ueki, C. Sasaki, Y. Yamada, T. Taguchi, K. Tadatomo, H. Okagawa, and H. Kudo, "Internal quantum efficiency of highly-efficient $In_xGa_{1-x}N$-based near-ultraviolet light-emitting diodes," *Appl. Phys. Lett.*, vol. 83, 4906, 2003.
[13] G. Chen, M. Craven, A. Kim, A. Munkholm, S. Watanabe, M. Camras, W. Götz, and F. Steranka, "Performance of high-power III-nitride light emitting diodes," *Phys. Status Solidi A*, vol. 205, 1086, 2008.
[14] K. A. Bulashevich, V. F. Mymrin, S. Y. Karpov, I. A. Zhmakin, and A. I. Zhmakin, "Simulation of visible and ultraviolet group-III nitride light emitting diodes," *J. Comput. Phys.*, vol. 213, 214, 2006.
[15] Y. Chen, P. Kivisaari, M.-E. Pistol, and N. Anttu, "Optimization of the short-circuit current in an InP nanowire array solar cell through opto-electronic modeling," *Nanotechnology*, vol. 27, 435404, 2016.
[16] O. Heikkilä, J. Oksanen, and J. Tulkki, "Ultimate limit and temperature dependency of light-emitting diode efficiency," *J. Appl. Phys.*, vol. 105, 093119, 2016.
[17] A. Haug, "Relations between the T_0 values of bulk and quantum-well GaAs," *Appl. Phys. B*, vol. 44, 151, 1987.
[18] W. Shockley and W. T. Read, Jr. "Statistics of the Recombinations of Holes and Electrons," *Phys. Rev.*, vol. 87, 835, 1952.
[19] S. Krishnamurthy and M. A. Berding, "Full-band-structure calculation of Shockley-Read-Hall recombination rates in InAs," *J. Appl. Phys.*, vol. 90, 848, 2001.
[20] O. Demichel, M. Heiss, J. Bleuse, H. Mariette, and A. Fontcuberta i Morral, "Impact of surfaces on the optical properties of GaAs nanowires," *Appl. Phys. Lett.*, vol. 97, 201907, 2010.
[21] R. B. Darling, "Defect-state occupation, Fermi-level pinning, and illumination effects on free semiconductor surfaces," *Phys. Rev. B.*, vol. 43, 4071, 1991.
[22] Y. Chen, P. Kivisaari, M.-E. Pistol, and N. Anttu, "Optimized efficiency in InP nanowire solar cells with accurate 1D analysis," *Nanotechnology*, accepted for publication. DOI: 10.1088/1361-6528/aa9e73
[23] Y. P. Varshni, "Temperature dependence of the energy gap in semiconductors," *Physica*, vol. 34, 149, 1967.
[24] P. J. L. Herve and L. K. J. Vandamme, "Empirical temperature dependence of the refractive index of semiconductors," *J. Appl. Phys.*, vol. 77, 5476, 1995.
[25] J. S. Blakemore, "Semiconducting and other major properties of gallium arsenide," *J. Appl. Phys.*, vol. 53, R123, 1982.

[26] C. Hauswald, I. Giuntoni, T. Flissikowski, T. Gotschke, R. Calarco, H. T. Grahn, L. Geelhaar, and O. Brandt, ”Luminous Efficiency of Ordered Arrays of GaN Nanowires with Subwavelength Diameters,” *ACS Photonics*, vol. 4, 52, 2017.

[27] M. Kantner and T. Koprucki, ”Numerical simulation of carrier transport in semiconductor devices at cryogenic temperatures,” *Opt. Quant. Electron.*, vol. 48, 543, 2016.

[28] M. Boroditsky, I. Gontijo, M. Jackson, R. Vrijen, and E. Yablonovitch, ”Surface recombination measurements on III-V candidate materials for nanostructure light-emitting diodes,” *J. Appl. Phys.*, vol. 87, 3497, 2000.

[29] F. Feix, T. Flissikowski, K. K. Sabelfeld, V. M. Kaganer, M. Wölz, L. Geelhaar, H. T. Grahn, and O. Brandt, ”Ga-Polar (In,Ga)N/GaN Quantum Wells Versus N-Polar (In,Ga)N Quantum Disks in GaN Nanowires: A Comparative Analysis of Carrier Recombination, Diffusion, and Radiative Efficiency,” *Phys. Rev. Appl.*, vol. 8, 014032, 2017.

[30] J. Oksanen and J. Tulkki, ”Drooping as a simple characterization tool for extraction efficiency and optical losses in light emitting diodes,” *Appl. Phys. Lett.*, vol. 97, 131105, 2010.